Research on Motion of the Flying Playing Card

S.T. Yau High School Science Award (Asia) research paper

Registration number: Phy-042

Name of team member: Liu Tianchi
School: Hwa Chong Institution
City, Country: Singapore, Singapore

Name of team member: Yu Shuhuai
School: Hwa Chong Institution
City, Country: Singapore, Singapore

Name of team member: Feng Linxuan
School: Hwa Chong Institution
City, Country: Singapore, Singapore

Name of supervising teacher: Dr Erkan Polatdemir
Position: Lecturer in physics
School/Institution: Hwa Chong Institution
City, Country: Singapore, Singapore

August 31, 2020

Commitments on Academic Honesty and Integrity

We hereby declare that we

1. are fully committed to the principle of honesty, integrity and fair play throughout the competition.
2. actually perform the research work ourselves and thus truly understand the content of the work.
3. observe the common standard of academic integrity adopted by most journals and degree theses.
4. have declared all the assistance and contribution we have received from any personnel, agency, institution, etc. for the research work.
5. undertake to avoid getting in touch with assessment panel members in a way that may lead to direct or indirect conflict of interest.
6. undertake to avoid any interaction with assessment panel members that would undermine the neutrality of the panel member and fairness of the assessment process.
7. observe all rules and regulations of the competition.
8. agree that the decision of YHSA(Asia) is final in all matters related to the competition.

We understand and agree that failure to honour the above commitments may lead to disqualification from the competition and/or removal of reward, if applicable; that any unethical deeds, if found, will be disclosed to the school principal of team member(s) and relevant parties if deemed necessary; and that the decision of YHSA(Asia) is final and no appeal will be accepted.

Name of team member: Liu Tianchi 刘天驰

Name of team member: Feng Linxuan 冯林萱

Name of team member: Yu Shuhuai 俞舒怀

Name of supervising teacher: Dr Erkan Polatdemir

Noted and endorsed by

Name of deputy school principal: Mr Tan Pheng Tiong

Acknowledgement

We would like to sincerely thank Dr Erkan Polatdemir from Hwa Chong Institution and the staff in the Science Research Centre of Hwa Chong Institution for mentoring us and providing us with necessary guidance.

Abstract

A standard playing card, of size $8.80cm \times 6.30cm$ and material plastic-coated paper, can travel a very long distance provided that spin is imparted as it is thrown. The motion of the card is primarily determined by the initial linear velocity, spinning angular velocity, and angle of attack. The aim of the research is to investigate the effects of these parameters on the distance travelled and trajectory of a playing card, and to explain the effects from both qualitative and quantitative approaches. After conducting experiments and computational simulation, we reached the conclusions that the deflection of the shape has a positive relationship with the spinning angular velocity and a negative relationship with the attack angle; and distance travelled has a positive relationship with the initial linear velocity and a negative relationship with the attack angle. Also, a simplified motion model has been established with certain premises.

Keywords: Playing cards, Magnus effect, Turbulent flow, Gyroscope stability, Computational fluid dynamics.

Contents

Introduction

1.1 Background

Throwing playing cards, which was first introduced in the West by stage magicians in the 19th century, has gained new popularity on the Internet these days. Videos shooting this phenomenon have millions of views. However, there is relatively little scientific documentation on the factors affecting the trajectory of the playing card and the distance it traveled. The complication of analysis mainly comes from the aerodynamic aspect.

1.2 Literature Review

White (1979) uses the case of a flat plate in a laminar flow as a typical example for analysing aerodynamic force. However, in our case, the spinning motion of the playing card may have effects on the aerodynamic force.

Amor Pilon (2015) concludes that although differences are observed, the behaviors of the flow for both flat plate and smooth rotating disk with or without roughness are almost identical. This assists our understanding of the case when the angle of attack is zero. However, when the attack angle is introduced, such approximation might not be valid due to the violation of symmetry.

Jiang et al. (2011) researches on and obtains approximate formulas for the calculation of the lift and drag coefficients for flat plates with large attack angles, which are applicable to our research's experiments. This simplifies our equation for calculation of aerodynamic forces acting on the flying playing card significantly.

Cross (2014) gives the conditions for both the positive Magnus effect and negative Magnus effect. This would be helpful to us in analysing the deflection of the shape.

Glenn Research Center (2013) published the calculation of Kutta-Joukowski lift for a cylinder. This provides us with a possible approach to calculate the Magnus force on the playing card.

White (1979) points out that when Mach number is less than 0.3, air can be deemed as incompressible fluid. This simplifies the analysis significantly.

Additionally, White (1979) also states that Reynold's number can be a good indicator of whether a laminar flow or turbulent flow is the real case. However, when an attack angle is introduced, the calculation of Reynold's number in this case is alien, and existing calculation cannot be adopted directly. Also, other than the Reynold's number, disturbance accounts for the formation of turbulence. This makes designing our experiments more challenging.

Launder and Spalding (1983) points out that the extensive list of unmeasurable unknowns in the original k-epsilon model is minimised by adopting the standard k-epsilon turbulent model. Thus, adopting the standard k-epsilon model provides us with insights of the turbulent flow in the case where the attack angle is large.

Scarborough (1958) explains the gyroscope stability and gyroscope equation. This could be helpful in explaining the inclination of the card in air and possible deflection in the trajectory of the card. However, a more quantitative analysis in this case is needed.

Theory

2.1 Laminar and turbulent flow

We will start off by analyzing the airflow over a non-rotating flat plate. As shown in the figure below, airflow over the front region of the plate is steady, and a laminar flow boundary is developed. In the transition region, airflow becomes unsteady due to the chaotic oscillation of the air molecules, and it eventually becomes completely turbulent. In order to investigate the effect of turbulence on the motion of the playing card, it is necessary to consider small eddy flows which occur in the turbulent region on the card into consideration.

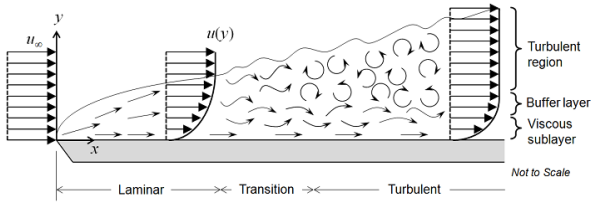

Figure 2.1: Flow of air over a flat plate

The spinning motion adds complexity to the problem. The spinning of the card may cause the airflow to be more chaotic and result in the formation of vortexes in our model. Magnus effect, which has a significant impact on the motion of the card, may also occur due to the rotation motion of the card.

2.2 Air resistance

As the mass of a playing card is measured to be $1.75 * 10^{-3}(kg)$, air resistance has a significant impact on the motion of the card. The magnitude of air resistance can be described by the following formula:

$$F = \frac{\rho A C_d}{2} v^2 \tag{2.1}$$

where ρ is the fluid density (kg/m^3), A the area pressed by air (m^2), C_d the drag coefficient, and v the speed of the object (m/s). In the case of playing card, the drag coefficient is hard to determine

due to its changing angular speed and attack angle. The bending of the card and turbulent flows around the card may also cause value change in the drag coefficient.

2.3 Magnus Effect

It is observed that a rotating card experiences deflection during its motion, and we will explain this phenomenon using the Magnus effect. As the ratio of the peripheral velocity of the edge of the spinning playing card, $v = 16\pi(rad/s) * 0.0755(m) = 3.79(m/s)$, to the linear velocity of the playing card, $u = 7.5m/s$, is around 0.569, greater than the threshold value of 0.5, positive Magnus effect should be observed.

On a cylinder, the force due to rotation is known as Kutta-Joukowski lift, which is given by

$$\frac{F}{L} = \rho v G \tag{2.2}$$

where $G = 2\pi r^2\omega$, L is the thickness (m), ω the angular speed (rad/s), ρ the fluid density (kg/m^3), v the speed of the object (m/s) and r the radius of the cylinder (m). In the following calculation, r of the playing card is taken as the geometry mean of the card's half length and half width, so $r = 5.56 * 10^{-3}(m)$

Thus, given the velocity and angular velocity of the card, the force produced by the Magnus effect can be calculated.

2.4 Reynolds Number

Reynolds number (Re number) helps to determine the behaviour of the airflow. At low Re number, airflow is more likely to be dominated by laminar flow while at high Re number, airflow is more likely to be turbulent.

Re number can be calculated as:

$$Re = \frac{\rho u L}{\mu} = \frac{uL}{v} \tag{2.3}$$

where ρ is the density of the fluid (kg/m^3), u the flow speed (m/s), L a characteristic linear dimension (m), μ the dynamic viscosity of the fluid (Pa/s), and v the kinematic viscosity of the fluid (m^2/s).

In the case of a playing card, $\mu = 4.0(Pa/s), L = 0.0755(m), v = 1.48*10^{-5}(m^2/s)$. So, $Re = 20405$, which turbulent flow is dominant unless stabilizing effects are introduced. As a result, $k-\epsilon$ turbulent model is chosen for our model.

2.5 $K-\epsilon$ Turbulent Model

The most general form of Navier-Stokes equations is given as:

$$\frac{\partial \rho}{\partial t} + \nabla \cdot (\rho \mathbf{u}) = 0 \tag{2.4}$$

$$\rho \frac{\partial \mathbf{u}}{\partial t} + \rho(\mathbf{u} \cdot \nabla)\mathbf{u} = \nabla \cdot [-p\mathbf{I} + \tau] + \mathbf{F} \tag{2.5}$$

$$\rho C_p \left(\frac{\partial T}{\partial t} + (\mathbf{u} \cdot \nabla)T \right) = -(\nabla \cdot \mathbf{q}) + \tau : \mathbf{S} - \frac{T}{\rho} \frac{\partial \rho}{\partial T}\bigg|_p \left(\frac{\partial p}{\partial t} + (\mathbf{u} \cdot \nabla)p \right) + Q \tag{2.6}$$

Where equation(2.4) represents the conservation of mass, equation(2.5) represents the conservation of kinetic energy and equation(2.6) represents the conservation of energy.

The equations can be simplified when the fluid is incompressible. The maximum initial linear velocity by human throwing is around $15.0(m/s)$, which is 0.04 Mach and is significantly smaller than the threshold value of 0.3. Thus, it is reasonable to assume air as incompressible in our experiments.

When the fluid is incompressible and Newtonian, Navier-Stokes equations take the form:

$$\begin{aligned} \rho \tfrac{\partial \mathbf{u}}{\partial t} + \rho(\mathbf{u} \cdot \nabla)\mathbf{u} &= \nabla \cdot \left[-p\mathbf{I} + \mu \left(\nabla \mathbf{u} + (\nabla \mathbf{u})^T \right) \right] + \mathbf{F} \\ \rho \nabla \cdot \mathbf{u} &= 0 \end{aligned} \tag{2.7}$$

The $k-\epsilon$ model includes two additional variables: the turbulent kinetic energy, k, and the turbulent dissipation rate, ε. The turbulent viscosity is:

$$\mu_T = \rho C_\mu \frac{k^2}{\varepsilon} \tag{2.8}$$

where C_μ is a experimental determined constant.
The transport equation for k is:

$$\rho \frac{\partial k}{\partial t} + \rho \mathbf{u} \cdot \nabla k = \nabla \cdot \left(\left(\mu + \frac{\mu_\mathrm{T}}{\sigma_k} \right) \nabla k \right) + P_k - \rho \varepsilon \tag{2.9}$$

where P_k is:

$$P_k = \mu_\mathrm{T} \left(\nabla \mathbf{u} : \left(\nabla \mathbf{u} + (\nabla \mathbf{u})^T \right) - \frac{2}{3} (\nabla \cdot \mathbf{u})^2 \right) - \frac{2}{3} \rho k \nabla \cdot \mathbf{u}$$

The transport equation for ε is:

$$\rho \frac{\partial \varepsilon}{\partial t} + \rho \mathbf{u} \cdot \nabla \varepsilon = \nabla \cdot \left(\left(\mu + \frac{\mu_\mathrm{T}}{\sigma_\varepsilon} \right) \nabla \varepsilon \right) + C_{\varepsilon 1} \frac{\varepsilon}{k} P_k - C_{\varepsilon 2} \rho \frac{\varepsilon^2}{k} \tag{2.10}$$

Though the derivation of above equations is beyond the scope of our research, it is worth mentioning

that these equations are used in computational fluid dynamics programs (CFDs) to calculate the numerical solutions to our aerodynamic models.

2.6 Gyroscope Stability and Precession

It is observed that a playing card falls quickly to the ground and performs tumbling motion when the angular velocity is low. In contrast, with high angular velocity, a card has a stable axis of rotation due to gyroscope stability: resistance of a rotating body to change its axis of rotation.

Angular momentum imparted when the card spins, as $L = I_z w = 8.0 * 10^{-5}$ (kgm^2/s), where $I_z = 1.71 * 10^{-6}$ (kgm^2) and $w = 15\pi$ (rad/s). As the card moves forward, air resistance force exerts torque on the card so the angular velocity of the card gradually decreases. With an estimated pressure difference of $0.1(Pa)$ when the card is flat, expected magnitude of torque τ would be in the order of magnitude 10^{-6}. Since $L > \tau$, the gyroscope stability provided by the spinning motion of the card mitigates the effects of disturbance of the air so the card is able to maintain a horizontal motion.

Also, precession is observed that the card spins about one axis and the net torque exerts on the card about a second axis, the spinning card will precess about the third axis as explained by the gyroscope equation. Formula will be:

$$\tau = \omega \times L \tag{2.11}$$

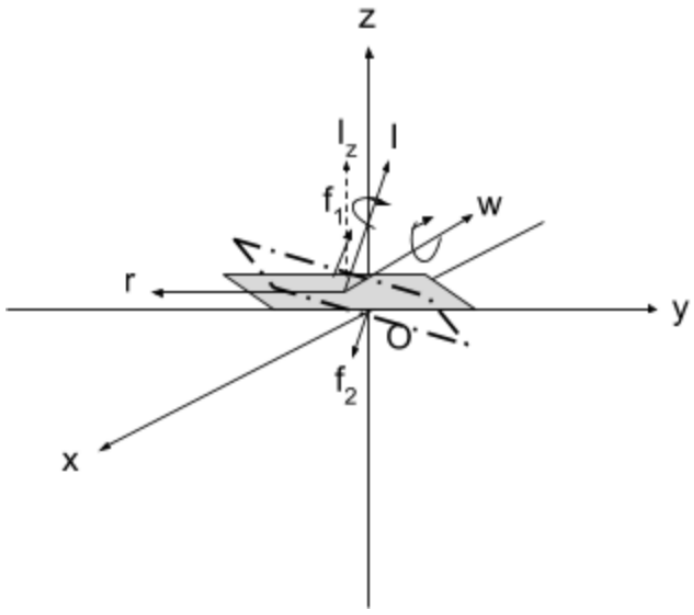

Figure 2.2: Precession of the card

Model

We chose COMSOL, a multiphysics stimulation platform, as our computation software. COMSOL uses Finite Element Method (FEM), breaking our model into small elements and repeating iterations to find solutions for our $k - \epsilon$ model.

3.1 CFDs model

A traditional way of analysing the aerodynamic effect of an object is to put the object in a wind tunnel. We build our model under similar condition as shown in the following diagram:

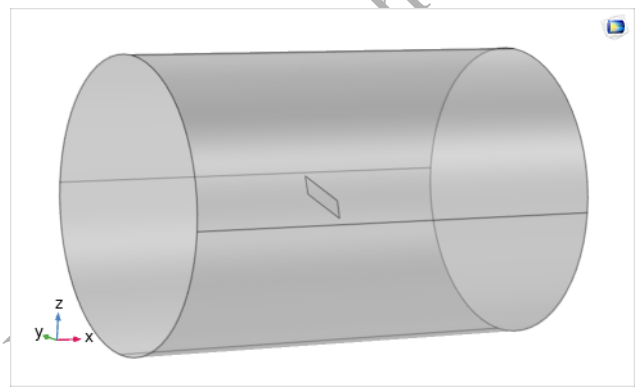

Figure 3.1: Model Setup

In the model, the playing card is placed in the middle with an attack angle of 45° to the x-axis. A uniform airflow of velocity $2.5(m/s)$ enters from the left inlet. The direction of the flow is from left to the right and is parallel to the x-axis. Additionally, the air density is taken as $1.183(kg/m^3)$, while the viscosity of air is taken as $1.81 * 10^5(Pa/s)$. The standard atmosphere pressure is used in our computation.

3.1.1 Lift Force on the Card

The resultant streamlines of the airflow when the velocity is 2.5 (m/s), attack angle is 45°, and angular velocity is 10π (rad/s), are shown as below:

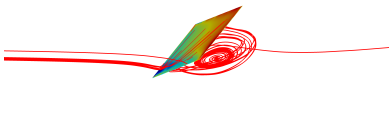

Figure 3.2: Side view

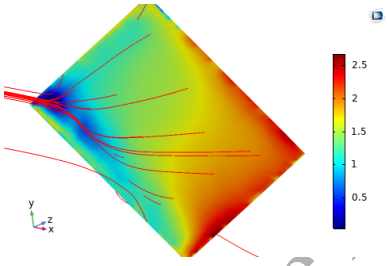

Figure 3.3: Front view

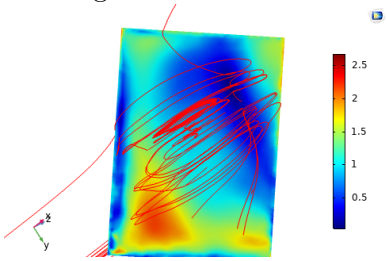

Figure 3.4: Back view

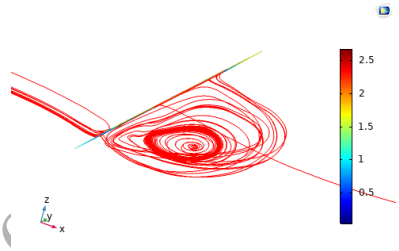

Figure 3.5: Display of the vortex

The card is rotating in an anti-clockwise direction when viewed from above. From Figure 3.3, the velocity of the streamlines of air is at its minimum at the corner where the card cuts the airflow. However, as shown in Figure 3.4, the average velocity of streamlines is even slower at the back side of the card. By Bernoulli's principle, a pressure difference between the playing card's upper and lower surface is produced which will provide lift force for the playing card. Since the magnitude of the streamline filed is uneven, a torque is produced which subsequently reduces the playing card's angular velocity.

The lift force can be further explained by investigating the vortex shown in the Figure 3.5. The playing card experiences a vortex lift effect as the card flows over the vortex and is pulled inwards and downwards, generating the lift force.

3.1.2 Constants Determination

Many constants are derived through COMSOL simulation. The derived values of the constants are then used in the construction of rigid body motion model. Due to the chaotic nature of playing card model, a slight change in variables may result in significant change in the card's motion obtained. Moreover, variables such as the attack angle, the initial velocity of the card, or the pressure difference keep changing during the motion. In order to simplify our calculation, slight changes in the value of variables are not taken into account in our model calculation, and the value of constants

are averaged to minimise errors.

For instance, in order to determine the lift drag constant C_d, we set the attack angle to be 90° as shown by Figure 3.6 and Figure 3.7. By integrate the force acting on the card, the force opposing the movement of the card is measured. Substitute this into equation (2.1), then we can determine the value of C_d.

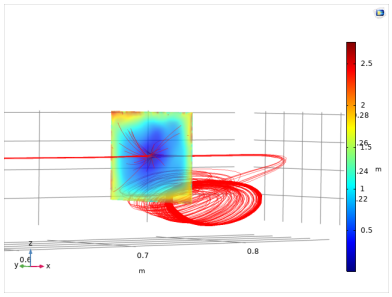

Figure 3.6: Side view (streamline)

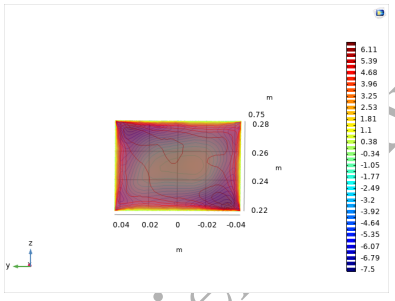

Figure 3.7: Front view (pressure)

A set of constants calculated is displayed below.

Variable	Description	Value
P	Average pressure difference	0.1 N/m^2
A	Pressure area on card	$5 * 10^{-4} m^2$
C_d	Drag coefficient	1.72
τ_0	Torque on the card in the rotation plane	$-1.7 * 10^{-6}$kgm^2

3.1.3 Assumptions

In our model, the playing card is considered as a rigid body, and we assume angular velocity has no effect on the air resistance force experienced by the playing card.

We will justify our assumption by proving that the bending of the playing card during its motion is insignificant and thus can be ignored. A standard playing card is made of paper coated with a layer of cellulose acetate polymer, or a layer of vinyl plastics. The young's modulus of paper ranges from 2.0 to 4.0(GPa)(azo, nd), while that of the cellulose acetate polymer and the vinyl polymers are between 2.4 and 4.1 (GPa)(vin, nd). Thus, a minimum Young's modulus value 2.0 (GPa) can be used for calculation of the maximum deformation of the playing card in flight. As shown by the following COMSOL simulation, expected maximum difference in the pressure between edges and the centre is 8.0(Pa) (when the wind velocity is 2.5(m/s), the attack angle is 45° and the angular velocity is $10\pi(rad/s)$; the playing card is rotating in anti-clockwise direction when viewed above the front).

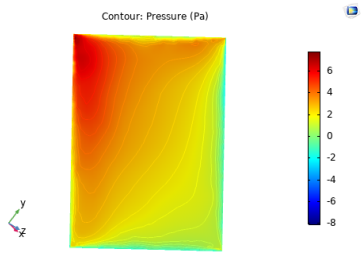

Figure 3.8: Pressure on the front

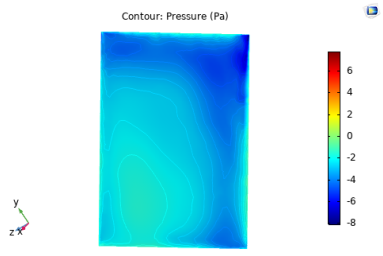

Figure 3.9: Pressure on the back

By calculation, the card's maximum deflection is $0.000247(m)$, which is negligible as compared to its half-length $(0.0440m)$ or half-width $(0.0315m)$. Thus, it is reasonable to consider the playing card as a rigid body in our modelling process. The calculation of the maximum deflection is given as:

$$y_{max} = -\frac{\alpha q b^4}{Et^3} \tag{3.1}$$

where E is Young's modulus, t is the plate thickness, α and β is the constant derived from table below(fla, nd), q is the load per unit area.

a/b	1.0	1.2	1.4	1.6	1.8	2.0	3.0	4.0	5.0	∞
β	0.2874	0.3762	0.4530	0.5172	0.5688	0.6102	0.7134	0.7410	0.7476	0.7500
α	0.0444	0.0616	0.0770	0.0906	0.1017	0.1110	0.1335	0.1400	0.1417	0.1421
γ	0.420	0.455	0.478	0.491	0.499	0.503	0.505	0.502	0.501	0.500

Figure 3.10: Table of value of α,β for different a/b values

We calculate the Resistance force experienced by the playing card when there is an angular acceleration as shown in the graph:

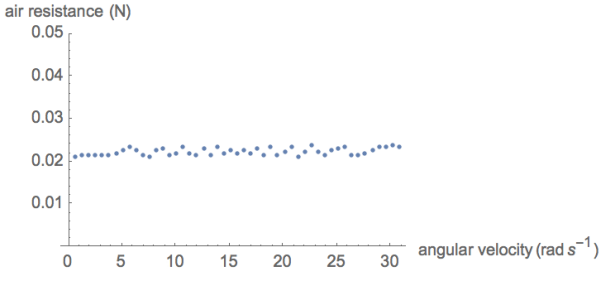

Figure 3.11: Plot of Air Resistance against Angular Velocity

Even though the angular velocity of the playing card is increasing, the change of the air resistance

is not significant. Thus, it is justified that the changes in angular velocity have insignificant effect on the air resistance experienced by the flying playing card.

3.2 Rigid Body Motion Simulation

We denote the launching direction as positive-x direction, counter-gravity direction as positive-z, and set up a Cartesian coordinate system according to right-hand rule. The displacement of the landing point of the card parallel to the y-axis reflects the distance travelled by the card, while the displacement parallel to the x-axis describes the shape of the trajectory. As the calculation of the aerodynamic forces for flat plate with large angles of attack is extremely complicated, and such scenarios are relevant to our focus to a small extent only, we do not discuss them. Instead, our main focus is on cases with small angles of attack which are less than 30°. In these cases, the drag force component is much more significant than the lift force component. Hence, only drag force component is included in our equations.

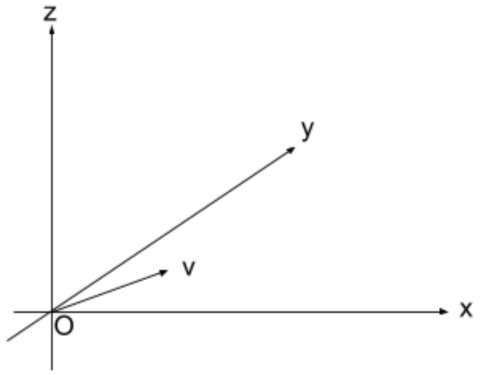

Figure 3.12: Tracker frame-by-frame analysis

3.2.1 Translational Motion

In x-direction, only air resistance force is concerned. By Newton's second law,

$$m\ddot{x}(t) = -0.5\rho C_d A \sin\theta(t)\dot{x}(t)^2 \tag{3.2}$$

In y-direction, only air resistance force is concerned. By Newton's second law,

$$m\ddot{y}(t) = -\rho C_d \dot{x}(t)\cos\theta(t)(2\pi r^2)(15\pi)(th)\cos\phi(t) \begin{cases} 0.5\rho C_d A \sin\theta(t)\dot{y}(t)^2 & \dot{y(t)} < 0 \\ -0.5\rho C_d A \sin\theta(t)\dot{y}(t)^2 & \dot{y(t)} \geq 0 \end{cases} \tag{3.3}$$

In z-direction, air resistance force and gravity are concerned. By Newton's second law,

$$m\ddot{z}(t) = -mg + \begin{cases} 0.5\rho C_d 2A\cos\theta(t)\cos\phi(t)\dot{z}(t)^2 & \dot{z(t)} < 0 \\ -0.5\rho C_d 2A\cos\theta(t)\cos\phi(t)\dot{z}(t)^2 & \dot{z(t)} \geq 0 \end{cases} \tag{3.4}$$

3.2.2 Rotational Motion

With the aid of the concept of Euler angle, we define the rotation about x-axis as ϕ, the rotation about y-axis as θ, the rotation about z-axis as α.

Also, when calculating the moment of inertia, I_z is normally calculated as $M(a^2+b^2)/12$. Then, for I_x and I_y, since the card is spinning at high speeds, I_x and I_y are approximately the same. By applying perpendicular axis theorem, each is half of I_z.

For the rotation about x-axis, only the torque by aerodynamic forces is concerned. By Newton's second law for rotation,

$$PAr\sin\theta(t) = I_{xy}\ddot{\theta(t)} \tag{3.5}$$

For the rotation about y-axis, precession and torque by aerodynamic forces are concerned. By Newton's second law for rotation,

$$I_z(\dot{\alpha(t)}\dot{\phi(t)}) - PAr\sin\phi(t) = I_{xy}\ddot{\phi(t)} \tag{3.6}$$

For the rotation about z-axis, only the torque by aerodynamic forces is concerned. By Newton's second law for rotation,

$$I_z\ddot{\phi(t)} = -\tau_0 \tag{3.7}$$

3.2.3 Initial Condition

To solve the differential equations numerically, for the 6 unknowns in the equations, 12 initial conditions are required.

$$\begin{array}{cc} x(0) = 0 & \dot{x(0)} = v_0\cos\theta_0 \\ y(0) = 0 & \dot{y(0)} = 0 \\ z(0) = 1.25 & \dot{z(0)} = v_0\sin\theta_0 \\ \theta(0) = \theta_0 & \dot{\theta(0)} = 0 \\ \phi(0) = 0 & \dot{\phi(0)} = 0 \\ \alpha(0) = 0 & \dot{\alpha(0)} = \omega \end{array} \tag{3.8}$$

where v stands for initial linear velocity (m/s), θ_0 stands for the attack angle, and ω stands for the spinning angular velocity (rad/s). The initial velocity in the z direction is not zero because a force is applied in the z direction by the rubber band to shoot the card.

Experiment

4.1 Experimental Set-up

The experiments were conducted in the physics laboratory of the Science Research Centre of Hwa Chong Institution. The ventilations were switched off and motions were minimised to ensure a relatively breezeless condition as close as possible where still air could be assumed to hold.

4.1.1 Launching Device

Our launching device is designed as follows: a retort stand is secured to the horizontal surface by a G-clamp. Two boss clamps are then secured onto the retort stand, with one used to fix the acrylic card holder and the other used for fixing the rubber band. When launching, the rubber bands are pulled back and the length pulled is measured using a ruler with a precision of 0.1 centimeters. The rubber band is then released, subsequently hitting the edge of the playing card and imparting an angular velocity as well as a linear velocity to the card.

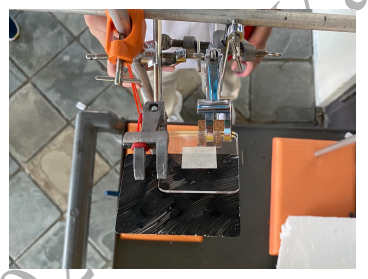

Figure 4.1: Top view

Figure 4.2: Front view

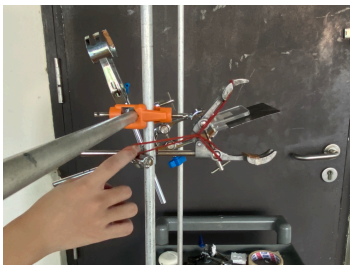

Figure 4.3: Side view

During experimentation, variables are varied as follows: the initial linear velocity is varied by using different number of rubber bands to vary the force during collision, and hence the energy imparted and initial linear velocity obtained; the spinning angular velocity is varied by adjusting the point of contact between the released rubber band the playing card; lastly, the angle of attack

is varied by adjusting the angle between the card holder and the horizontal. The above mentioned methods are, at the same time, used to control the respective variables.

To ensure the reliability of the data collected, we adopted the following methods. All playing cards used are identical, ensuring a consistent mass of the card in each experiment. The cards are new and completely flat, minimising the possibility of disturbing the air. Rubber bands used are also identical to ensure a constant spring constant. The force exerted by the spring at the instant of contact is therefore directly proportional to the stretch of the rubber band, enabling us to use the lengths of elongation of the rubber band as an indication of the relative initial linear velocity imparted.

4.1.2 Refinement of Data Collection Process

To facilitate the processing of data, all playing cards are coloured with one side black and the other side red for the purpose of clear tracking in the subsequent frame-by-frame analysis of video. Multiple white boards are set at the background of the video to better contrast the playing card in motion.

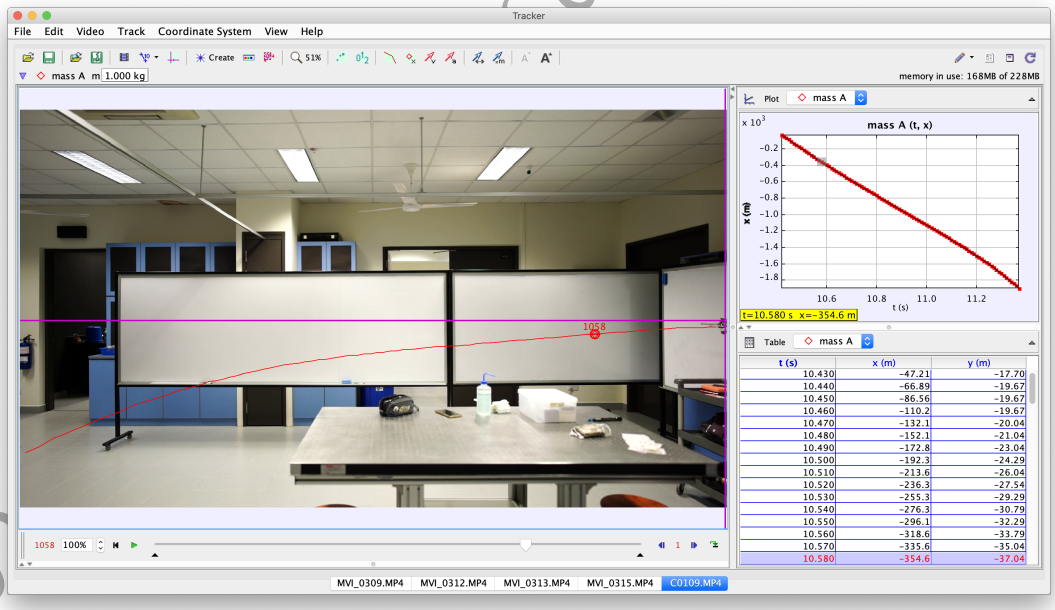

Figure 4.4: Tracker frame-by-frame analysis

Two cameras with high frame rates of 100 frames per second are used, with one installed at the front of the launching device collecting front views, and the other installed at the side collecting side views. The relatively high fps enables us to capture the motion of the cards in small time intervals.

4.2 Qualitative Experimental Data Analysis

The frame-by-frame analysis in Tracker is used to identify the position of the playing card and measure the initial linear speed and spinning angular velocity of the playing card, while Mathematica is used to point-plot the trajectory.

The Cartesian coordinate system used in our data analysis has the same orientation the coordinate system constructed preciously in the rigid body motion simulation.

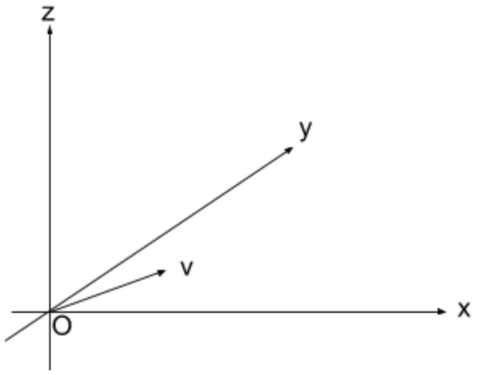

Figure 4.5: Figure of Cartesian coordinate system

In our analysis, deflection is represented by the displacement of the playing card's landing point parallel to the x-axis, while the distance travelled refers to the displacement of the card parallel to the y-axis.

For each set of experimental variables, we conduct five sets of experiments to collect consistent sets of data. The data is then averaged and used as the representative data for the specific condition.

4.2.1 Changing Spinning Angular Velocity

As shown in the graph, distance traveled is independent of the angular spinning velocity, while the deflection in trajectory has a positive relationship with the angular spinning velocity.

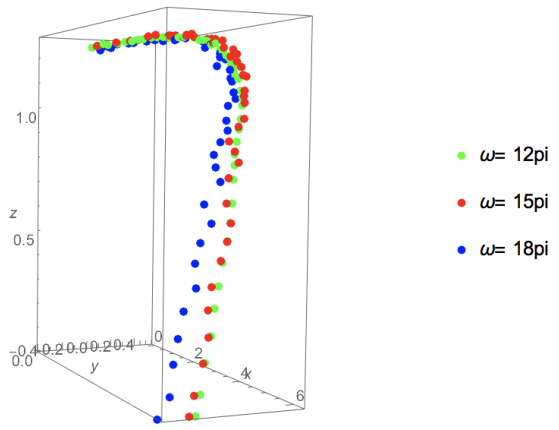

Figure 4.6: Trajectories with different initial spinning angular velocities

4.2.2 Changing Initial Linear Velocity

As shown in the graph, distance traveled has a positive relationship with the initial linear velocity, while the trajectory is independent of the initial linear velocity.

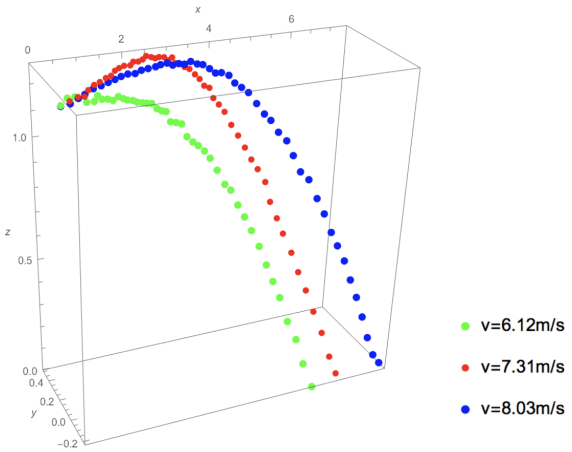

Figure 4.7: Plot of Air Resistance against Angular Velocity

4.2.3 Changing Attack Angle

As shown in the graph, distance traveled has a negative relationship with the angle of attack, while the deflection in trajectory has a positive relationship with the attack angle.

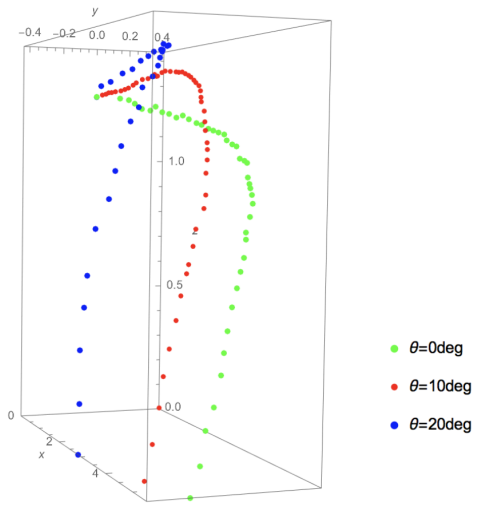

Figure 4.8: Trajectories with different angles of attack

4.3 Comparison with Model

4.3.1 Result Analysis

For our experiments, due to the constraints of the launching device, a y-component velocity will be imparted to the card. This will be included in our initial conditions in the rigid body motion model.

Several sets of data are presented as follows:

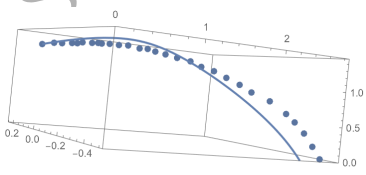

Figure 4.9: Data Set 1

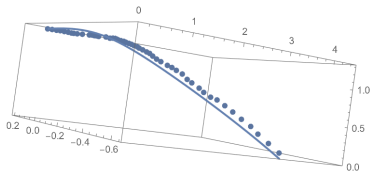

Figure 4.10: Data Set 2

As observed, the heights calculated by the model tends to be larger than the actual values and the calculated distance travelled tends to be smaller than the actual distance travelled. These could be because due to the constraints of the launching device, actual attack angle is smaller than expected,

leading to larger height reached and shorter period in air, subsequently smaller distance travelled.

Generally, the rigid body motion can be a good approximation with certain limitations.

4.3.2 Limitations

The model is only suitable for relatively small angles of attack, namely less than or equal to 30°, because when the attack angle is large, the calculation of air resistance is complicated with the turbulent flow situation.

Additionally, the model requires the spinning angular velocity to be larger than $10\pi(rad/s)$ so that a steady flight can be presumed as the gyroscope stability effect is more significant.

4.4 Error Analysis

4.4.1 Instability of Surrounding Air

The air is not absolutely still during our data collection process, as human movements and heat flow generates random motion of the air which could not be possibly eliminated.

4.4.2 Inaccuracy in Tracking

As frame-by-frame analysis in Tracker is utilised to obtain all measurements of the distance travelled by the card, the initial linear velocity, and the spinning angular velocity, the resolution of the frame images is crucial to ensure accuracy. However, due to resource limitations, we use cameras with high frame rate of 100 frames per second instead of high speed cameras which could capture images with a much higher frame rate of 250 frames per second. The relatively longer exposure time needed for the filming affects the quality of the frames, as the playing card continues its motion during the short time interval, leading to unclear edges of the card. As such, the centre of mass of the playing card has to be estimated during the tracking process, leading to a maximum uncertainty of 0.50 centimeters and hence a percentage uncertainty of 5.0%.

4.5 Improvement

4.5.1 Improving Launching Device

Below is our proposal for improvements of the launching device. The primary motor serves the purpose of adjusting the initial linear velocity by adjusting its rotating speed; the secondary motor adjusts the playing card's initial spinning angular velocity by adjusting its rotating speed; the attack angle can be adjusted by orientating the whole device at different angles. The part to launch the playing card has two layer, namely inner and outer layer. The playing card is fixed to the inner layer, and the outer layer can be pushed out to detach the card.

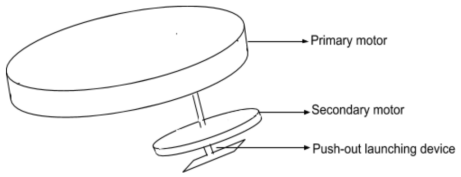

Figure 4.11: Diagram of the improved design

Another possible design is proposed by the Youtuber Mark Rober. The computer-aided design is shown in the figure below. The card deck is underneath the bottom of the launching device. The first belt and a pulley then, slide cards forward to the front of the machine one card at a time. A second belt, which is wrapped around an O ring and connected to a motor, is responsible for imparting the spin to the card. The initial linear velocity and the spinning angular velocity of the card can be changed by adjusting the variable resistors connected in the circuit, while the angle of attack can be varied by orienting the whole launching device to a particular angle to the horizontal level.(Mark Rober, 2018)

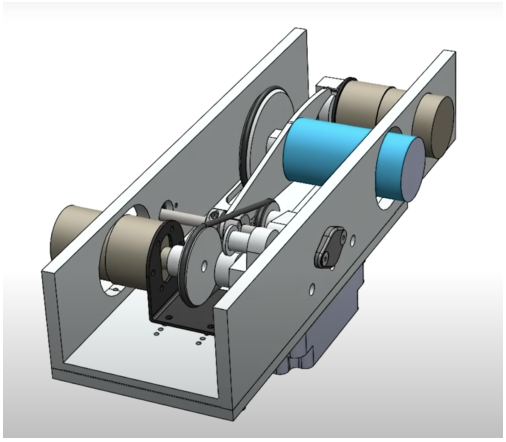

Figure 4.12: Possible design of launching device

4.5.2 Wind Tunnel Experiment

Currently, our research on aerodynamic forces is only based on CFD simulation while wind tunnel experiments are lacking. CFD might be a good approximation for most cases. However, its accuracy depends on the size of meshes. Hence, if a wind tunnel experiment can be carried out to determine the constants needed, the modelling can be more accurate.

Conclusion

1) The deflection of the trajectory is positively correlated to the spinning angular velocity, while it has a negative correlation with the attack angle. Initial linear velocity has insignificant effect on the shape of the trajectory.

2) The distance travelled is positively correlated to the initial linear velocity and a negative relationship with the attack angle. Spinning angular velocity has insignificant effect on the distance travelled by the card.

3) Also, a simplified motion model has been established with certain premises.

4) Tips for throwing the playing card far: horizontal launch, large initial linear velocity, and sufficient spinning angular velocity.

Bibliography

(n.d.). Cellulose acetate. Accessed Aug.25 2020.

(n.d.). Flat rectangular plate with all edges simply supported equations and calculator. Accessed Aug.25 2020.

(n.d.). Young's modulus - tensile and yield strength for common materials. Accessed Aug.25 2020.

Amor Pilon, J. M. (2015). Turbulent boundary layer: comparison between a flat plate and a rotating disk with and without periodic roughness.

Cross, R. (2014). Wind tunnel photographs.

Glenn Research Center (2013). Lift of a rotating cylinder.

Jiang, H., Cao, S., and Cheng, Z. (2011). Lift and drag coefficients of flow around a flat plate at high attack angles. *Chinese Journal of Applied Mechanics*, 5.

Launder, B. E. and Spalding, D. B. (1983). The numerical computation of turbulent flows. In *Numerical prediction of flow, heat transfer, turbulence and combustion*, pages 96–116. Elsevier.

Mark Rober (2018). Playing card machine gun-card throwing trick shots. [YouTube video]. Accessed Aug.31 2020.

Scarborough, J. B. (1958). *The Gyroscope*. Interscience Publ.

White, F. M. (1979). *Fluid mechanics*. Tata McGraw-Hill Education.

Appendix

A.1 Mathematica Code for the Model

```
In[1219]:= rule={m->0.00175,P1->0.1,P2->0.1,A1->0.0005,A2->0.0005,v->7,g->9.81,
A->0.005544,Con->1.72,\[Rho]->1.293,r->0.0556,th->0.00027,Ixy->0.00000085407,
Iz->0.00000170814,torque->6.3 10^-5}

position=
NDSolve[{

m x''[t]==-0.5 \[Rho] Con (A Sin[\[Theta][t]]) (x'[t])^2,
m y''[t]==If[y'[t]<0, 0.5 \[Rho] Con (A Sin[\[Phi][t]]) (y'[t])^2,
-0.5 \[Rho] Con (A Sin[\[Phi][t]])(y'[t])^2]
-\[Rho] x'[t] Cos[\[Theta][t]] (2 Pi r^2 15 pi th) Cos[\[Phi][t]],
m z''[t]==-m g + If[z'[t]<0,
0.5 \[Rho] 2 (A Cos[\[Theta][t]] Cos[\[Phi][t]]) (z'[t])^2,
-0.5 \[Rho] Con (A Cos[\[Theta][t]] Cos[\[Phi][t]]) (z'[t])^2],
P1 A1 r Sin[\[Theta][t]]==Ixy \[Theta]''[t],
Iz(\[Phi]'[t]\[Phi]''[t])-P2 A2 r Sin[\[Phi][t]]==Ixy \[Phi]''[t],
Iz \[Alpha]''[t]==-torque,

\[Theta][0]==Pi/18,
\[Theta]'[0]==0,
\[Phi][0]==0,
\[Phi]'[0]==0,
x[0]==0,
x'[0]==v Cos[\[Theta][0]],
y[0]==0,
y'[0]==0.17,
z[0]==1.25,
\[Alpha][0]==0,
\[Alpha]'[0]==16 Pi,
z'[0]==v Sin[\[Theta][0]]

}/.rule,{x,y,z,\[Theta],\[Phi],\[Alpha],\[Alpha]'},{t,0,1.27},
MaxStepSize->0.0001]

Out[1219]= {m->0.00175,P1->0.1,P2->0.1,A1->0.0005,A2->0.0005,v->7,g->9.81,
A->0.005544,Con->1.72,\[Rho]->1.293,r->0.0755,th->0.00027,Ixy->8.5407*10^-7,
Iz->1.70814*10^-6,torque->0.000063}
Out[1220]= {{x->InterpolatingFunction[Domain: {{0.,1.27}}
Output: scalar

],y->InterpolatingFunction[Domain: {{0.,1.27}}
Output: scalar
```

```
],z->InterpolatingFunction[Domain: {{0.,1.27}}
Output: scalar

],\[Theta]->InterpolatingFunction[Domain: {{0.,1.27}}
Output: scalar

],\[Phi]->InterpolatingFunction[Domain: {{0.,1.27}}
Output: scalar

],\[Alpha]->InterpolatingFunction[Domain: {{0.,1.27}}
Output: scalar

],\[Alpha]^\[Prime]->InterpolatingFunction[Domain: {{0.,1.27}}
Output: scalar

]}}
In[1169]:= a=Import["/Users/liutianchi/Desktop/10␣deg␣zui␣xin␣.xlsx"]

In[1221]:= xx=x/.position[[1,1]]
yy=y/.position[[1,2]]
zz=z/.position[[1,3]]
\[Theta]\[Theta]=\[Theta]/.position[[1,4]]
\[Phi]\[Phi]=\[Phi]/.position[[1,5]]
Out[1221]= InterpolatingFunction[Domain: {{0.,1.27}}
Output: scalar

]
Out[1222]= InterpolatingFunction[Domain: {{0.,1.27}}
Output: scalar

]
Out[1223]= InterpolatingFunction[Domain: {{0.,1.27}}
Output: scalar

]
Out[1224]= InterpolatingFunction[Domain: {{0.,1.27}}
Output: scalar

]
Out[1225]= InterpolatingFunction[Domain: {{0.,1.27}}
Output: scalar

]
In[1226]:= FindRoot[zz[t]==0,{t,0.7}]
Out[1226]= {t->1.03444}
In[1227]:= Show[{ListPointPlot3D[a,PlotRange->Automatic],
ParametricPlot3D[{xx[t],yy[t],zz[t]},{t,0,1.0344351444781088‘},
PlotRange->Automatic]}]
```